Lawrence Berkeley National Laboratory
LBL Publications

Title
Reversible Emulsions from Polyoxometalate—Polymer: A Robust Strategy to Cyclic Emulsion Catalysis and High-Internal-Phase Emulsion Materials

Permalink
https://escholarship.org/uc/item/21w4t4ck

Journal
Journal of the American Chemical Society, 145(46)

ISSN
0002-7863

Authors
Wan, Chuchu
Wu, Yutian
Cheng, Quanyong
et al.

Publication Date
2023-11-22

DOI
10.1021/jacs.3c10005

Copyright Information
This work is made available under the terms of a Creative Commons Attribution License, available at https://creativecommons.org/licenses/by/4.0/

Peer reviewed

eScholarship.org Powered by the California Digital Library
University of California

Reversible Emulsions from Polyoxometalate–Polymer: A Robust Strategy to Cyclic Emulsion Catalysis and High-Internal-Phase Emulsion Materials

Chuchu Wan,[1†] Yutian Wu,[1†] Quanyong Cheng,[1] Xiang Yu,[1] Yuhang Song,[1] Chengshu Guan,[1] Xuemei Tan,[1] Caili Huang,[1,*] Jintao Zhu,[1] and Thomas P. Russell[2,3*]

1. Key Laboratory of Materials Chemistry for Energy Conversion and Storage of Ministry of Education (HUST), School of Chemistry and Chemical Engineering, Huazhong University of Science and Technology (HUST), Wuhan 430074, China
2. Department of Polymer Science and Engineering, University of Massachusetts, Amherst, Massachusetts 01003, United States
3. Materials Sciences Division, Lawrence Berkeley National Laboratory, Berkeley, California 94720, United States

ABSTRACT: Reversible Pickering emulsions, achieved by switchable, interfacially-active colloidal particles, that enable on-demand emulsification/demulsification or phase inversion, hold substantial promise for biphasic catalysis, emulsion polymerization, cutting fluids, and crude oil pipeline transportation. However, particles with such responsive behavior usually require complex chemical syntheses and surface modifications, limiting their extensive use. Herein, we report a simple route to generate emulsions that can controllably and reversibly undergo phase inversion. The emulsions are prepared and stabilized by the interfacial assembly of polyoxometalate (POM)–polymer, where their electrostatically interact at the interface is dynamic. The wettability of the POMs that dictates the emulsion type, can be readily regulated by tuning the number of polymer chains bound to POMs, that, in turn, can be controlled by varying the concentrations of both components and the water/oil ratio. In addition, the number of polymer chains anchored to the POMs can be varied by controlling the number of negative charges on the POMs by an *in situ* redox reaction. As such, a reversible inversion of the emulsions can be triggered by switching between exposure to ultraviolet (UV) light and introduction of oxygen (O_2). Combining the function of POM itself, a cyclic interfacial catalysis system was realized. Inversion of the emulsion also affords a pathway to high-internal-phase emulsions (HIPEs).The diversity of the POMs, the polymers, and the responsive switching groups open numerous new, simple strategies for designing a wide range of responsive soft matter for cargo loading, controlled release, and delivery in biomedical and engineering applications without time-consuming particle syntheses.

KEYWORDS: reversible emulsion, POM–polymer assemblies, redox responsiveness, cyclic catalysis, HIPEs

INTRODUCTION

Pickering emulsions are droplets of one liquid dispersed in a second immiscible liquid that are stabilized by colloidal particles, as opposed to traditional surfactants or block copolymers.[1,2] The adsorption of particles to the oil−water interface is irreversible, since the reduction in the interfacial energy per particle is large, due to the size of the particles. This strong binding energy per particle prevents droplet coalescence, stabilizing the emulsions.[3-6] This stability coupled with the dense packing of the particles at the interface imparts robust mechanical properties to the emulsions, enabling applications in the food, cosmetics, and pharmaceutical industries.[7-9] For some applications emulsions with a transient stability are desirable, e.g., with interfacial catalysis, where demulsification or phase inversion is needed to easily extract products from the continuous phase.[4,10-13] If one could reversibly realize a phase inversion or de-emulsification, product separation and catalyst recovery would be facilitated.[14-16] Reversible emulsion manipulation, therefore, could significantly impact multiphase catalysis, emulsion polymerization, and froth flotation for the purification of precious mineral extracts.[17,18]

Tuning the hydrophilicity/hydrophobicity ratio of particles by changing their surface wettability has emerged as the most convenient and effective method to build controllable emulsions, where hydrophilic particles preferentially stabilize o/w emulsions while hydrophobic particles form w/o emulsions. Molecular adsorption or chemical grafting of stimuli-responsive small molecules or polymers onto the surface of the particles allows for tailoring hydrophilic/hydrophobic properties, that can be switched by external stimuli, like temperature,[19,20] CO_2,[21] pH,[22-24] magnetic field,[25,26] redox,[27] ions,[28] or light[14,29]. Kosif *et al.* designed Au nanoparticles (NPs) decorated with ligands having acid-labile tetrahydropyranyl (THP) ether chain-ends as stabilizers for acid-responsive emulsions. The *in situ* phase inversion from w/o to o/w emulsions was achieved as the Au NPs were

converted from oil-dispersible to water-dispersible by cleaving the labile chain-end by introducing acid. Unfortunately, the transition was irreversible.[30] Li *et al.*[15] achieved the reversible transition between emulsification and demulsification of a light-responsive emulsion based on Pd-supported silica particles modified by azobenzene ionic liquid molecules. The phase behavior was attributed to the *trans*- (relatively less polar) and *cis*- (relatively more polar) isomers of azobenzene groups triggered by UV/visible light affecting the adsorbed amount of ionic liquid molecules onto the particles and thus determining whether the particles can be stably adsorbed to the interface. Chen *et al.*[14] proposed another reversible phase inversion of a light-triggered emulsion by using photochromic spiropyran-grafted functional particles as emulsifiers, where the spiropyran can be reversibly switched between the hydrophobic, ring-closed spiropyran and the hydrophilic, ring-opened zwitterionic merocyanine with near-infrared (NIR)/visible light. With this method, product recovery, catalyst and emulsifier recycling were easily realized, significantly advancing sustainable chemical engineering. Although progress has been made in reversible emulsions, complex chemical syntheses and surface modifications of responsive ligand functionalized particles pose an impediment to their further development. Consequently, designing a simple method to realize reversible emulsions is needed.

From the point of view of the size of the particles, the binding energy of particles to the interface increases with the square of the particle radius. Microparticles have a strong binding energy to the interface, several orders of magnitude greater than thermal energy, $k_B T$, that benefits to the stabilization of emulsions but, on the other hand, requires careful control over their wetting characteristics to realize a reversible phase inversion (i.e., significant changes to the hydrophilic/hydrophobic properties).[22,25] Nanoparticles (NPs) with diameters of ~ 10 nm have binding energies that are comparable to thermal energy and, as such, their interfacial assemblies are dynamic with constant adsorption and

desorption of the NPs to the interface and cannot stabilize emulsions .[6,31] A range of tunable electronic, optical and catalytic properties of NPs make them attractive, if the binding energy can be increased.

Here, we report a simple strategy to realize redox-switchable reversible emulsions by tailoring the co-assembly of functional POMs with polymers having a complementary functionality at the oil–water interface. The negatively charged POMs are dissolved in water, while the amine-terminated polydimethylsiloxanes (PDMS-NH_2) are dissolved in toluene, and the two electrostatically interact at the interface, forming POM–polymer assemblies. The number and distribution of the anchored polymers across the surface of the POM dictates its wettability and the type of emulsion stabilized. As such, emulsion inversion was realized by adjusting the concentration ratio of the POM in the aqueous phase and the PDMS-NH_2 in toluene, or the water/oil mixing ratio. The surface properties of POMs can be altered to mediate the self-assembly behavior. A typical redox POM—phosphomolybdic acid (PMA, diameter ~ 1.1 nm), was selected, where the number of negative charges can be enhanced by UV light exposure, that will return to its original state upon interacting with O_2. With these redox reactions of PMAs, the emulsions stabilized by the PMA–PDMS-NH_2 assemblies can be reversibly changed between o/w and w/o. Such reversible emulsion inversion was further conducted on the cyclic catalytic oxidative desulfurization of benzothiophene (BT), along with product separation. The light-induced emulsion inversion affords a new strategy for the preparation of high-internal-phase emulsions (HIPEs, dispersed phase volume fraction over 74%) and related porous materials. By circumventing complex particle syntheses, our strategy opens exciting new avenues to advanced, responsive soft matter for remotely controlled delivery vehicles and release of encapsulated cargo.

RESULTS AND DISCUSSION

Before utilizing PMA–polymer assemblies to stabilize emulsions, the interfacial assembly kinetics of PMA and PDMS-NH_2 at the water–toluene interface were investigated by the time evolution of the interfacial tension (γ) using a pendant water droplet within an oil phase. Dissolved in water, $H_3PMo_{12}O_{40}$ is stable and is a discrete anion with 3 negative charges on its surface (balanced by countercations), usually written as $[PMo_{12}O_{40}]^{3-}$. $[PMo_{12}O_{40}]^{3-}$ is not active at the water–toluene interface (Figure S1), due to the inherent negative charge of the interface,[32] where the γ between an aqueous solution of $[PMo_{12}O_{40}]^{3-}$ and toluene is 33.5 mN m^{-1}, close to that between pure water and toluene of 36 mN m^{-1}. PDMS-NH_2 (molecular weight, MW = 2,000 g mol^{-1}), dissolved in toluene on the other hand, assembles into a monolayer at the interface, reducing γ to 30 mN m^{-1} within 500 s at a PDMS-NH_2 concentration of 0.02 mM (Figure S1). With PMA (0.05 mg mL^{-1}) in the aqueous phase, a very rapid reduction in γ to 17 mN m^{-1} was observed (Figure 1a), indicating that the negatively charged $[PMo_{12}O_{40}]^{3-}$ electrostatically interacts with protonated PDMS-NH_2, i.e., PDMS-NH_3^+, where the pH of PMA aqueous solution is ~ 4.0 and the pK_a of $-NH_2$ is ~ 9,[33] forming a monolayer of PMA–polymer assemblies at the interface (Figure S2).[34] In a typical PMA–polymer system, when the concentration of the PDMS-NH_2 solution was varied and the aqueous solution of PMA was fixed at 0.05 mg mL^{-1}, the initial rate at which the γ decreased was found to increase with increasing PDMS-NH_2 concentration and γ reached lower value. Above a concentration of 0.2 mM, γ did not decrease further and remained constant at ~ 15 mN m^{-1}. If, on the other hand, as the concentration of PMA was increased from 0.005 mg mL^{-1} to 1 mg mL^{-1} with a fixed PDMS-NH_2 concentration of 0.02 mM, the results in Figure 1b were obtained. For low concentration of PMA (0.005 mg mL^{-1}), the reduction in γ was gradual, with γ decreasing to 27 mN m^{-1}. As the concentration of PMA was increased, the reduction in γ was much more rapid, and γ decreased to 11 mN m^{-1}. This behavior demonstrates the dependence of

the assembly kinetics on the concentration of both components. It should also be noted that the initial rapid reduction in γ was followed by a second, slower process that leads to a continued slight decrease in γ with time. This slow process can be attributed to the rearrangement of the PMA–PDMS-NH_2 assemblies at the interface to increase the areal density.

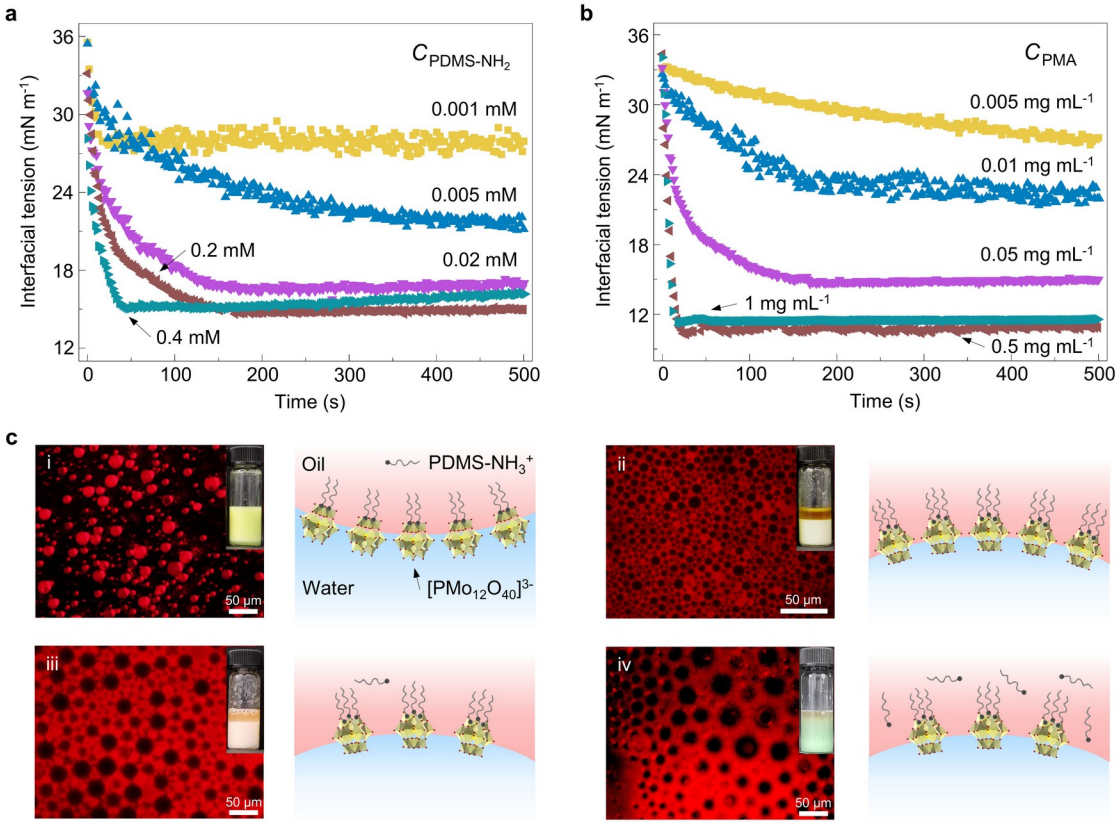

Figure 1. (a) Dynamic interfacial tension of 0.05 mg mL^{-1} PMA aqueous solution in contact with a toluene solution of PDMS-NH_2 at different concentrations. (b) Dynamic interfacial tension for a fixed concentration of PDMS-NH_2 (0.02 mM) with an increasing concentration of PMA from 0.005 to 1 mg mL^{-1}. (c) Emulsions prepared by the combination of PMA aqueous solution and PDMS-NH_2 toluene solution at different conditions: (i) [PMA] = 20 mg mL^{-1}, [PDMS-NH_2] = 10 mM, water/oil ratio is 5:5 (*v*/*v*); (ii) [PMA] = 20 mg mL^{-1}, [PDMS-NH_2] = 40 mM, water/oil ratio is 5:5 (*v*/*v*); (iii) [PMA] = 5 mg

mL^{-1}, [PDMS-NH_2] = 10 mM, water/oil ratio is 5:5 (*v*/*v*); (iv) [PMA] = 20 mg mL^{-1}, [PDMS-NH_2] = 10 mM, water/oil ratio is 3:7 (*v*/*v*). The oil phase was stained with Nile red (0.01 mM).

Having quantified the kinetic profiles for PMA–PDMS-NH_2 assembly, the formation and stabilization of emulsions was investigated. Neither PMA or PDMS-NH_2 stabilized emulsions (Figure S3), as would be expected. When agitated, equal-volume mixtures of aqueous solutions of PMA and PDMS-NH_2 solutions in toluene formed emulsions. The emulsified systems coalesced rapidly at low concentration of either PMA (2 mg mL^{-1} for a fixed concentration of PDMS-NH_2 (40 mM)) or PDMS-NH_2 (0.5 or 2 mM for a fixed concentration of PMA (5 mg mL^{-1})) (Figure S4), where PMA–PDMS-NH_2 assemblies show extreme hydrophobicity (a number of PDMS-NH_2 chains attached on one PMA) or hydrophilicity (PMAs anchored few PDMS-NH_2 chains), corresponding to the slow reduction in and higher ultimate value of γ (Figure 1a,b). Increasing the PMA or PDMS-NH_2 concentration to a critical value, e.g., 5 mg mL^{-1} PMA for a fixed concentration of PDMS-NH_2 (40 mM), resulted in stable emulsions.

Insight into the formation and control of these stable emulsions was obtained by investigating the parameters that govern the emulsion type and droplet size. We first considered a system formed from equal-volume mixtures of 20 mg mL^{-1} PMA aqueous solution and solution of 10 mM PDMS-NH_2 in toluene. Typical o/w droplets were observed (Figure 1c(i)). If the concentration of PMA aqueous solution is fixed, and that of PDMS-NH_2 in toluene increased to 40 mM and, a w/o emulsion was observed (Figure 1c(ii)). This phase inversion arises from the variation in the wettability of PMAs by attaching more PDMS-NH_2 chains that leads more hydrophobic characteristics. The increase in PDMS-NH_2 concentration resulted in the reduction in droplet size from 18.5 ± 2.1 to 8.4 ± 1.1 μm, which arises from the increased interfacial area that is stabilized in these emulsions. The dramatic decrease of the electrical conductivity (from 1955 to 0.011 μS cm^{-1}) provided further evidence of the emulsion inversion. If, on the other hand, the

concentration of PDMS-NH_2 was fixed at 10 mM and the PMA concentration reduced to 5 mg mL^{-1}, a transition to a w/o emulsion occurred as well (0 μS cm^{-1}) (Figure 1c(iii)), where the droplet diameter increased to 21.5 ± 2.2 μm due to a decrease in the amount of interfacial assemblies. The phase inversion was also induced by lowering the volume ratio of water and oil to 3:7 with the fixed concentrations of PMA aqueous solution (20 mg mL^{-1}) and PDMS-NH_2 toluene solution (10 mM) (Figure 1c(iv)). This was accompanied by an increase in droplet size (32.9 ± 5.1 μm). This transition can be attributed to the decrease in the PMA/PDMS-NH_2 ratio that yields more hydrophobic PMAs, and the increase in the volume fraction of the oil phase, tending to invert the continuous phase. To demonstrate these, we conducted two control experiments. First, the emulsions were prepared such that the volume ratio of water and oil was 5:5, and the concentrations of PMA aqueous solution and PDMS-NH_2 in the toluene were 12 (= $20 \times \frac{3}{5}$) mg mL^{-1} and 14 (= $10 \times \frac{7}{5}$) mM, respectively, having the same ratio of PMA/PDMS-NH_2 with the system in Figure 1c(iv). Second, 33 (≈ $20 \div \frac{3}{5}$) mg mL^{-1} PMA aqueous solution and 7 (≈ $10 \div \frac{7}{5}$) mM PDMS-NH_2 solution in toluene were used to generate emulsions with a volume ratio at 3:7, where they kept the same ratio of PMA/PDMS-NH_2 with the sample in Figure 1c(i). Emulsion inversion was observed for both cases by controlling one of the variables (Figure S5a,b).

On the basis of the dynamic assembly behavior of PMA–PDMS-NH_2, tailor made emulsions were produced by engineering either one component of these two or both simultaneously, or the water/oil mixing ratio. *In situ* changing the attributes of one component, especially photolytically, capitalizing on controlling the number of negative

charges on the surface of the PMAs, affords a straightforward, practical means to customize their emulsion behavior. We assessed the redox-responsive properties of PMAs, that can be photochemically reduced in the presence of an electron (e^-) donor, such that they have more negative charges, and be reoxidized in air or by use of any of a number of oxidizing agents.[35-39] A water-soluble *O*-(2-Aminoethyl)polyethylene glycol (PEG-NH_2, MW = 3,000 g mol^{-1}) was used here, as the e^- donor (derived from protonated amine group on the polymers, i.e., $-NH_3^+$), providing a model molecule to redox responsively interact with the PMA. The PMA aqueous solution (containing PEG-NH_2) had a light yellow color with no obvious absorption from 380–800 nm wavelength. After UV irradiation for 15 min, the solution changed to a blue color, a characteristic of the valence of Mo (V) or Mo^{5+},[38,40,41] with a proton and charge transfer mechanism between PMA molecule and $-NH_3^+$ species (Scheme S1).[35,36] This had a broad absorption in the visible centered at ~ 660 nm (Figure S6). Pumping in O_2 (1 h) converted the appearance and absorption spectrum of the solution back to the pristine state along with the return of the Mo atoms to VI or Mo^{6+}.[35,36]

To quantify the impact of the Mo atom valence on the surface charge properties of PMAs, we used X-ray photoelectron spectroscopy (XPS) to probe the details of the redox processes. Zooming in the spectra, where the sample was prepared from aqueous solution of PMA and PEG-NH_2, allows us find the binding energy level of the 3d orbital of Mo (Mo_{3d}) in PMAs (Mo^{6+}) decomposed into two spin-orbitals of $3d_{5/2}$ and $3d_{7/2}$ with peaks at 231.49 and 234.69 eV, respectively (Figure S7).[42] Two new shoulder peaks at 230.18 and 233.29 eV appeared for the sample prepared from the solution after UV irradiation that are assignable to the $3d_{5/2}$ and $3d_{7/2}$ levels of Mo^{5+}, respectively. The ratio between integral area of the peaks at 230.18 and 231.49 eV, i.e., $A_{230.18}/A_{231.49}$, after peak-differentiation, or $A_{233.29}/A_{234.69,}$ is 0.51. This demonstrates that around one third of the Mo atoms were converted from Mo^{6+} to Mo^{5+} in the PMAs, resulting in an average of 7 negative charges

on the surface of PMAs after reduction (based on the assumption that one PMA molecule carries 15 negative charges on its surface if all Mo atoms are reduced[39]). The characteristic peaks for Mo^{5+} disappeared as the sample was oxidized by O_2. Zeta potential of PMA aqueous solution after photoreduction and subsequent oxidation changed from -39.4 to -66.9 and to -42.2 mV (Figure S8), providing further evidence for the enhancement and return of the number of negative charges on the surface of PMAs in these processes.

We next examined the programmable interfacial assembly behavior of PMA with PDMS-NH_2 and their stabilized emulsions that are produced by the *in situ* triggered change on PMAs. Here, we began with o/w emulsions prepared from equal volumes of 20 mg mL^{-1} solution of PMA in water and a 10 mM solution of PDMS-NH_2 in toluene. Upon UV irradiation (5 min of exposure at 365 nm) and re-emulsification, the emulsions were inverted to the w/o type (Figure 2a). As demonstrated above, UV irradiation led to an increase in the number of negative charges on the surface of PMAs, such that more PDMS-NH_2 chains can anchor to the PMAs. Consequently, the phase inversion can be attributed to the increased hydrophobicity of PMA–PDMS-NH_2 assemblies. Bubbling O_2 into the emulsions led to the oxidation of PMAs, allowing the w/o emulsions return to o/w emulsions. Replacing O_2 with nitrogen (N_2) as a control, yielded no change (Figure S9). The reversibility of the emulsion inversion was highly repeatable, without substantial change to the emulsion morphology in 3 cycles for each corresponding point (Figure S10).

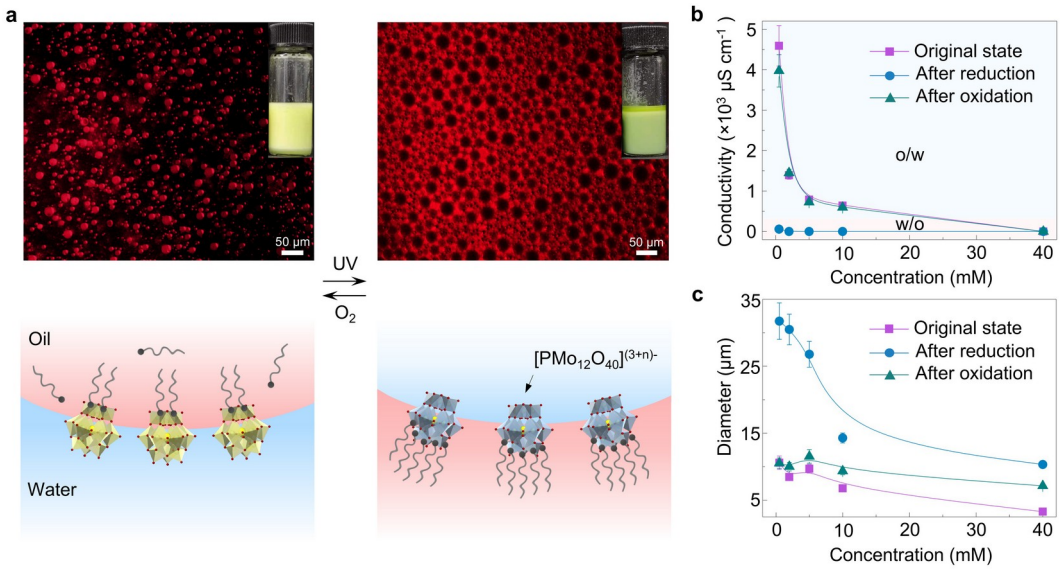

Figure 2. (a) Macroscopic and fluorescence microscopy images of reversible emulsions achieved by PMA–PDMS-NH_2 assemblies through UV light/O_2 triggers. [PMA] = 20 mg mL^{-1}, [PDMS-NH_2] = 10 mM, water/oil ratio is 5:5 (*v*/*v*). (b) Conductivity of emulsions stabilized by 20 mg mL^{-1} PMA aqueous solution and PDMS-NH_2 toluene solution with varying concentrations (0.5–40 mM) in a redox process. Water/oil ratio is 5:5 (*v*/*v*). (c) Average droplet diameter of emulsions stabilized by 20 mg mL^{-1} PMA aqueous solution and PDMS-NH_2 toluene solution with varying concentrations (0.5–40 mM) in a redox process. Water/oil ratio is 5:5 (*v*/*v*).

To investigate the influence of the PMA/PDMS-NH_2 ratio on the redox-induced emulsion inversions, we prepared a series of emulsions from equal volumes of a 20 mg mL^{-1} aqueous solution of PMA and toluene solutions of PDMS-NH_2 varying the concentration from 0.5–40 mM. In keeping with the results in Figure 1c, for concentrations of PDMS-NH_2 $\leq$ 10 mM, o/w emulsions were found, while at higher concentration of PDMS-NH_2 (40 mM), w/o emulsions were found (Figure S11). For lower concentration of PDMS-NH_2, fewer polymer chains anchored to the PMAs at the interfaces, leading to a greater hydrophilicity of the interfacial assemblies, a higher conductivity and a larger droplet size (Figure 2b,c). Decreasing the concentration of

PDMS-NH_2 to 0.2 mM prevented emulsion formation. Upon exposure to UV light, w/o emulsions formed even though the PMA–PDMS-NH_2 assemblies have strong hydrophilic characteristics for the case of 0.5 mM PDMS-NH_2 (Figure S11), where the conductivity of the emulsions decreased to near zero and the size of droplets increased several times (e.g., for a 0.5 mM concentration of PDMS-NH_2, the conductivity decreased from 4590 to 0.058 μS cm^{-1} and the droplet size increased from 10.6 ± 1.0 to 31.7 ± 2.7 μm). The increase in the droplet size arises, more than likely, from the increased electrostatic repulsion between PMAs at the interface that causes the separation distance between PMAs to increase. Subsequent oxidation (by injecting O_2) caused the emulsions invert to the o/w state. However, the emulsion droplets were larger than those in the original emulsions. This may arise from the relatively weaker emulsifying ability for the *in situ* changed interfacial assemblies compared to the pristine ones.

These reversibly switchable emulsions, are well-suited for biphasic cyclic catalysis and product separation, since PMAs not only act as interface immobilizers (assisted by polymer ligands) but also are effective catalysts for many reactions (e.g., esterification of benzoic acid and butane-1-ol, Diels–Alder reaction of quinone, and oxidation of ethylene to acetic acid). The oxidation of sulfide compounds to sulfone products was selected as a model example (Figure 3a), since the removal of sulfur in fuel oils is an environmentally important topic, it undergoes conventionally complex multi-step operations, and it characteristically has low efficiency.[43] For a typical experiment, an *n*-octane solution (1 mL) of benzothiophene (BT, a typical sulfur compound, 100 ppm) and PDMS-NH_2 (10 mM) was mixed with the aqueous phase (1 mL) containing PMA (20 mg mL^{-1}) and hydrogen peroxide (H_2O_2, *ca.* 0.24 mg mL^{-1}, slightly higher than stoichiometry) to give o/w emulsions. The oxidation reaction of BTs (in the dispersed oil phase) took place at the interfaces using PMA as the catalyst with the participation of oxidizing agent H_2O_2 in water. The emulsions were stirred at 40 °C. The reaction process was monitored by

UV−vis spectroscopy by analyzing the oil phase that was collected after centrifugation and subsequent extraction with dimethyl formamide (DMF) at different reaction stages (Figure 3b). Pure BTs show four characteristic absorption peaks at 269, 280, 289, and 298 nm. As the reaction proceeded, the characteristic adsorption of BTs became weaker. The UV−vis spectra of the DMF solution had a broad adsorption from 265 to 340 nm and its intensity leveled off, corresponding to the adsorption of the oxidation products. The reaction was completed in 4 h. The S, S-dioxide product, benzothiophene 1,1-dioxide (BTDO), was verified by nuclear magnetic resonance (NMR) results (Figure S12). The oxidation conversion of BTs to BTDOs, or the sulfur removal efficiency (S_0-S_t/S_0), where S_0 and S_t are the BT content in the extracted oil phase at time 0 h and t h, respectively, was determined using a fluorescent UV sulfur analyzer and plotted as a function of reaction time (Figure 3c). The sulfur removal reached 90.7% after reaction time of 4 h, which was far superior to that of the planar oil−water interfacial catalysis (no more than 45% after 4 h reaction), indicating the superiority of the emulsion process for biphasic catalysis and product extraction or removal. The BT removal value is likely to be related to the extraction efficiency rather than the catalytic reaction. Therefore, the extraction with DMF on centrifuged *n*-octane solution was further conducted three times and, the BT removal reached up to 99.6%, meaning that 0.4 ppm BTs was left.

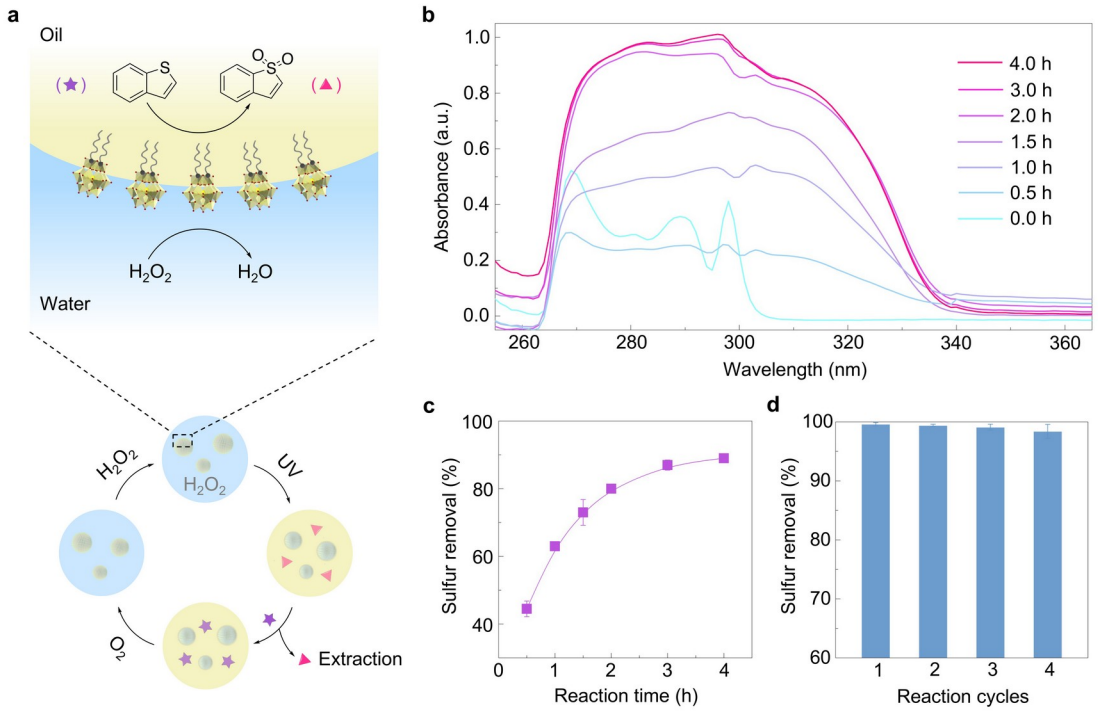

Figure 3. (a) Schematic illustration showing a redox-switchable reversible emulsion for cyclic catalytic oxidative desulfurization of BT. (b) UV−vis spectra of DMF solution extracting the reacting oil phase once (equal volume) over reaction time. (c) Sulfur removal of the reacting oil phase extracted once by equal volume of DMF as a function of reaction time. (d) Sulfur removal of the oxidized oil extracted 3 times by equal volume of DMF in 4 cycles.

Aside from extracting the oxidation products from the centrifuged oil, analyzing the interfacial catalysis, and collecting related compounds can be achieved by inverting the o/w emulsions into w/o emulsions. Specifically, an emulsion system prepared with the same parameters in Figure 3c was irradiated by UV light for 5 min after completing the catalysis reaction (4 h). Subsequently, the emulsion was converted to w/o type with re-emulsification and the microscopic morphology is similar to the middle sample in Figure S4a, containing 0.55 mL of a nearly clear upper oil phase and 1.45 mL bottom stable emulsion. The oil was carefully extracted and rinsed three times with fresh *n*-octane. The oil was then extracted with DMF solvent three times and, concentrated to around 1 mL to

allow the next step of oxidation product analysis. A removal yield of BTs (99.7%) was found (Figure 3d). Finishing the oxidation and product separation, refilling *n*-octane solution of BT (0.3 mg, keep total concentration still at 100 ppm) and PDMS-NH_2 (7.4 μmol, details about replenished stocks are given in the Catalytic Reaction Section in Supporting Information) to around 2 mL of total system was followed for the next cycle of sulfur removal. Before the second catalytic cycle, the w/o emulsion was inverted back to o/w emulsion by injecting O_2 and re-emulsification and, H_2O_2 (0.24 mg) was also added to the aqueous phase. As shown in Figure 3d, the BT removal was 99.6% with the same treatment methods of the first cycle for product separation. This value remained at 98.4% after four consecutive runs. Such a slight decrease was, more than likely, caused by the partial loss of the catalyst during the reaction cycle. This highly efficient and cyclable catalytic oxidative desulfurization not only avoids sophisticated catalyst design but also provides a simple strategy to streamline the oxidative desulfurization of fuel oil, in which the catalyst loss, filter blocking, intensive energy consumption of catalyst separation, and recycling (usually undergo centrifugation, filtration, and purification steps) are inevitable with homogeneous catalysis or conventional emulsion catalysis.

The controllable ability to invert these emulsions by adjusting the PMA/PDMS-NH_2 ratio by varying the concentrations of both components, the water/oil ratio, and the number of negative charges on the PMAs, affords a simple route to high-internal-phase emulsions (HIPEs), commonly referred to as super-concentrated emulsions, with a minimum internal-phase volume fraction of 0.74. These are widely used in food processing, pharmaceutical formulations owing to their tunable rheology, and tissue engineering and materials science as templates to generate highly porous materials.[44-46] We first produced a series of emulsions by mixing 20 mg mL^{-1} PMA aqueous solution and 10 mM PDMS-NH_2 toluene solution in various volume ratios (1:9–8:2), and then examined the responsive behavior of the emulsions upon exposure to UV trigger (Figure

S13). Consistent with the results in Figure 1c, the emulsions tended to be o/w for water/oil ratio ≥ 5:5. Exposure to UV light, the o/w emulsions were inverted to w/o for samples with water/oil ratios of 5:5 and 7:3, but not for samples with a water/oil ratio higher than 8:2. This inability of these emulsions to invert arises, more than likely, from the insufficient number of polymers to render the photoreduced higher charged PMAs hydrophobic. Increasing the concentration of PDMS-NH_2 to 100 mM, o/w emulsion was found when the water/oil mixing ratio is 8:2 (Figure 4a(i)) and, a stable inverted w/o HIPE was realized upon UV irradiation and re-emulsification (Figure 4b(i)), where close-packed w/o droplets were observed. The cryo-scanning electron microscopy (cryo-SEM) images further confirmed that the inverted w/o droplets were crowded and deformed, while initial o/w droplets were loosely distributed in the continuous phase (Figure 4a(ii),b(ii)). The compacted droplets in the continuous phase had significant impact on the viscoelasticity of the emulsion system, and, therefore, its processing.[44,45] Figure 4c shows the change in the elastic modulus (G') and viscous modulus (G'') of emulsions as a function of shear strain. In the case of original o/w emulsion, both G' and G'' showed low values (< 1.6 Pa), and G'' was consistently larger than G' at all strains, exhibiting fluid properties. For w/o HIPE, a linear viscoelastic region was observed at low strain values (< 0.25%), where G' and G'' depended only slightly on strain and G' (200.5 Pa) was dominant over G'' (56.6 Pa), which are hallmarks of elastic gel-like structures. In comparison to HIPEs stabilized by modified nanoparticles, HIPE covered with PMA–PDMS-NH_2 assemblies had significantly greater mechanical strength.[46] This can be attributed to the entanglement of polymer chains anchored to the PMAs that improves the adhesion and connectivity between the compacted droplets, resulting in the gel-like rheological behavior of the HIPE system.[47] For the shear strain over the linear viscoelastic region, G' gradually decreased. Above a critical strain (24.99%), G'' (69.8 Pa) became larger than G' (66.9 Pa), such that a solid-like to liquid-like transition occurred. The

viscosity curves of these two systems are shown in Figure 4d, as a function of shear rate. Compared to o/w emulsion having high fluidity with a shear-independent viscosity of 0.15 Pa·s, HIPE had high viscosity of 719 Pa·s at low shear rate of 0.1 s^{-1}. The value dropped rapidly and monotonically to 19.1 Pa·s at 10 s^{-1}, and finally leveled off (3.4 Pa·s) at higher shear rates, showing typical shear-thinning behavior where high shear stress destroys the entanglement of the polymer chains and even macrostructure of the compacted droplets. Such elastic characteristic and shear-thinning behavior of the HIPE system enable it to flow through a nozzle during pressure-driven extrusion and has adequate mechanical strength to withstand the layer stacking after extrusion, making it easy to process, as for example by 3D printing. As such, a rose-like sample was printed with HIPEs (Figure 4d). The HIPE inks have the potential to diversify the applications of 3D printing in foods, cosmetics, drug delivery systems, and packaging materials.

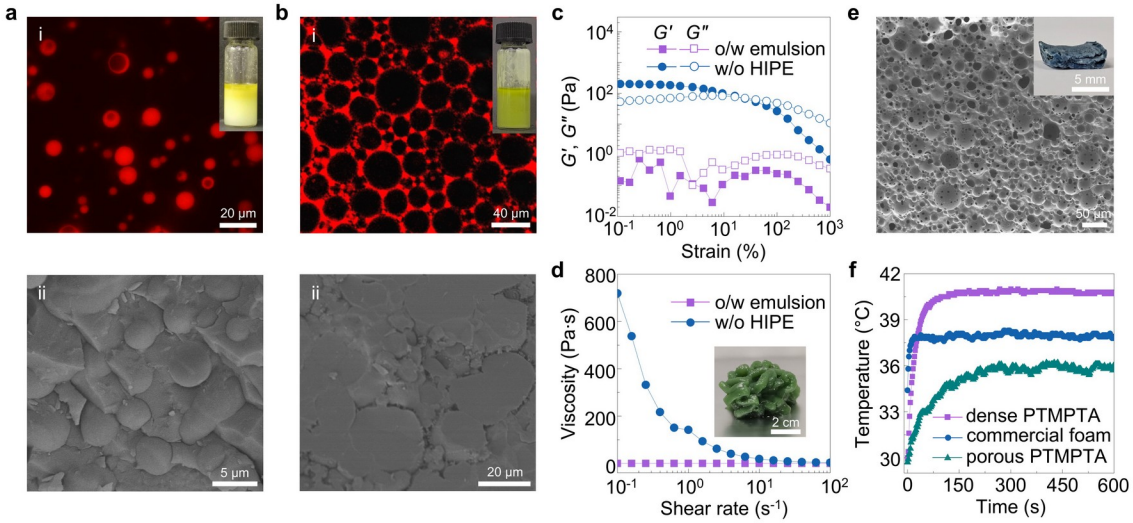

Figure 4. Macroscopic and fluorescence (i) and cryo-electron (ii) microscopy images of (a) original o/w emulsion and (b) inverted w/o HIPE. [PMA] = 20 mg mL^{-1}, [PDMS-NH_2] = 100 mM, water/oil ratio is 8:2 (*v*/*v*). (c) *G′* and *G″* as a function of shear strain of the corresponding emulsions shown in (a) and (b). The frequency is kept constant at 1 Hz. (d) Viscosity as a function of shear rate of the corresponding emulsions shown in (a) and (b). The strain is kept constant at 0.1%. Inset showing

extrusion-printed rose pattern with inverted w/o HIPEs. (e) Scanning electron microscope (SEM) image of HIPE-templated porous material. (f) The surface temperatures of porous PTMPTA with open cells, dense PTMPTA, and commercial thermal insulation foam on a hot stage over time.

Following the 3D printing of HIPEs, we prepared porous materials by polymerization and freeze-drying by adding (trimethylolpropane triacrylate, TMPTA, 20% *v*/*v* with respect to oil phase) and photoinitiators (2-hydroxy-2-methyl propiophenone, 1% *v*/*v*) to the oil phase. As shown in Figure 4e, the porous sample showed interconnected open-cell structures, where the pore size and shape were commensurate with the corresponding emulsion droplets. Such interconnected porous structures arise from the rupture of thin oil layers between compacted water droplets due to interfacial instabilities induced by temperature and concentration gradients during the polymerization.[48] We then investigated the thermal insulation of HIPE-templated porous materials—porous PTMPTA. Dense PTMPTA (polymerizing the monomers directly in oil) and commercial thermal insulation foam (chemically cross-linked polyethylene foam, XPE foam) with the same thickness were used for comparison. The time dependence of the surface temperature of the three samples was recorded when holding on a hot stage set at 42.2°C over time using a thermal imager. It was found that the porous PTMPTA had the largest temperature difference between the hot plate surface and the sample surface (6.4°C) after the surface temperature reached a constant value (~ 10 min), as shown in Figure 4f. In contrast, the surface temperature of the commercial foam and dense PTMPTA increased rapidly with smaller temperature differentials (4.3 and 1.5°C, respectively) with the hot plate. These results indicate that the porous structure with open cells contributes to excellent thermal insulation performance. This provides a simple method to expand the library for creating HIPEs or related materials, including the chemical selection of both interfacial immobilizers and mixing systems, since conventional means inevitably require either the delicate surface modification or detailed

synthesis of colloids to achieve a well-defined hydrophilic/hydrophobic ratio, allowing the stabilization of HIPEs. We note that achieving the correct hydrophilic/hydrophobic ratio is critical. The HIPE-templated materials described here may further find numerous applications as tissue scaffolds, sensor materials, supports for solid phase synthesis, and hydrogen storage.

CONCLUSIONS

In summary, a simple method to achieve tailor made emulsions was demonstrated by manipulating the co-assembly of PMA and PDMS-NH_2 at water/oil interfaces. Programming the concentration of the components in each phase or PMA's surface properties by a redox-switchable means to controllably and reversibly invert emulsions not only circumvents complex chemical syntheses and surface modifications of responsive particles to pursue diversified emulsions, but it is general and readily replaced by a wide range of nanoparticles, polymers, and responsive functionalities, well beyond the initial model described here. As a proof of concept, two applications based on the customized emulsion behavior were demonstrated, specifically, cyclable catalytic oxidative desulfurization by using the catalytic function of PMAs and the reversible emulsion inversion, and preparation of HIPEs and related porous thermal insulation materials based on the regulation of the morphology and mechanical properties. A broad range of applications is envisioned for these responsive soft matters or prescribed emulsion-based materials in cosmetics, coatings, nanomedicines, biomedical tissues, chemical engineering, and materials science by designing specific functionalities or stimuli for the nanoparticles and/or polymer ligands.

ASSOCIATED CONTENT

Supporting Information

Discussion of materials and characterization, testing for redox responsiveness of PMAs, preparation of emulsions and templated porous materials, catalytic reaction, mechanism of proton and charge transfer interaction, dynamic interfacial tension, droplet morphology, macroscopic and fluorescence microscopy images of emulsified samples, UV–vis absorption spectrum, XPS spectra, Zeta potential, NMR spectra, conductivity (PDF)

AUTHOR INFORMATION

Corresponding Authors

Caili Huang – *Key Laboratory of Materials Chemistry for Energy Conversion and Storage of Ministry of Education (HUST), School of Chemistry and Chemical Engineering, Huazhong University of Science and Technology (HUST), Wuhan 430074, China;* orcid.org/0000-0003-1209- 1141; Email: cailihuang@hust.edu.cn

Thomas P. Russell – *Department of Polymer Science and Engineering, University of Massachusetts, Amherst, Massachusetts 01003, United States; Materials Sciences Division, Lawrence Berkeley National Laboratory, Berkeley, California 94720, United States;* orcid.org/0000-0001- 6384-5826; Email: russell@mail.pse.umass.edu

Authors

Chuchu Wan – *Key Laboratory of Materials Chemistry for Energy Conversion and Storage of Ministry of Education (HUST), School of Chemistry and Chemical Engineering, Huazhong University of Science and Technology (HUST), Wuhan 430074, China*

Yutian Wu – *Key Laboratory of Materials Chemistry for Energy Conversion and Storage of Ministry of Education (HUST), School of Chemistry and Chemical Engineering, Huazhong University of Science and Technology (HUST), Wuhan 430074, China*

Quanyong Cheng – *Key Laboratory of Materials Chemistry for Energy Conversion and Storage of Ministry of Education (HUST), School of Chemistry and Chemical Engineering, Huazhong University of Science and Technology (HUST), Wuhan 430074, China*

Xiang Yu – *Key Laboratory of Materials Chemistry for Energy Conversion and Storage of Ministry of Education (HUST), School of Chemistry and Chemical Engineering, Huazhong University of Science and Technology (HUST), Wuhan 430074, China*

Yuhang Song – *Key Laboratory of Materials Chemistry for Energy Conversion and Storage of Ministry of Education (HUST), School of Chemistry and Chemical Engineering, Huazhong University of Science and Technology (HUST), Wuhan 430074, China*
Chengshu Guan – *Key Laboratory of Materials Chemistry for Energy Conversion and Storage of Ministry of Education (HUST), School of Chemistry and Chemical Engineering, Huazhong University of Science and Technology (HUST), Wuhan 430074, China*
Xuemei Tan – *Key Laboratory of Materials Chemistry for Energy Conversion and Storage of Ministry of Education (HUST), School of Chemistry and Chemical Engineering, Huazhong University of Science and Technology (HUST), Wuhan 430074, China*
Jintao Zhu – *Key Laboratory of Materials Chemistry for Energy Conversion and Storage of Ministry of Education (HUST), School of Chemistry and Chemical Engineering, Huazhong University of Science and Technology (HUST), Wuhan 430074, China*

Author Contributions

[†]C.W. and Y.W. contributed equally to this work.

Notes

The authors declare no competing financial interest.

ACKNOWLEDGMENTS

This work was supported by the National Natural Science Foundation of China (21903033, 22275063, and 52293474), the Fundamental Research Funds for the Central Universities (5003013050), and start-up funds from the Huazhong University of Science and Technology. Initial support from the Oak Ridge National Laboratories for C.H. is acknowledged. T.P.R. was supported by the U.S. Department of Energy, Office of Science, Office of Basic Energy Sciences, Materials Sciences and Engineering Division under Contract No. DE-AC02-05-CH11231 within the Adaptive Interfacial Assemblies Towards Structuring Liquids program (KCTR16).

REFERENCES

(1) Ramsden, W.; Gotch, F. Separation of Solids in the Surface-layers of Solutions and 'Suspensions' (Observations on Surface-membranes, Bubbles, Emulsions, and Mechanical Coagulation). —Preliminary Account. *Proc. R. Soc. London* **1904**, *72*, 156−164.

(2) Pickering, S. U. CXCVI. —Emulsions. *J. Chem. Soc. Trans.* **1907**, *91*, 2001−2021.

(3) Lin, Y.; Skaff, H.; Emrick, T.; Dinsmore, A. D.; Russell, T. P. Nanoparticle Assembly and Transport at Liquid–Liquid Interfaces. *Science* **2003**, *299*, 226−229.

(4) Zhang, M.; Wei, L.; Chen, H.; Du, Z.; Binks, B. P.; Yang, H. Compartmentalized Droplets for Continuous Flow Liquid–Liquid Interface Catalysis. *J. Am. Chem. Soc.* **2016**, *138*, 10173−10183.

(5) Furst, E. M. Directing Colloidal Assembly at Fluid Interfaces. *Proc. Natl. Acad. Sci.* **2011**, *108*, 20853−20854.

(6) Forth, J.; Kim, P. Y.; Xie, G.; Liu, X.; Helms, B. A.; Russell, T. P. Building Reconfigurable Devices Using Complex Liquid–Fluid Interfaces. *Adv. Mater.* **2019**, *31*, 1806370.

(7) Ikem, V. O.; Menner, A.; Horozov, T. S.; Bismarck, A. Highly Permeable Macroporous Polymers Synthesized from Pickering Medium and High Internal Phase Emulsion Templates. *Adv. Mater.* **2010**, *22*, 3588−3592.

(8) Peng, S.; Cao, F.; Xia, Y.; Gao, X.-D.; Dai, L.; Yan, J.; Ma, G. Particulate Alum via Pickering Emulsion for an Enhanced COVID-19 Vaccine Adjuvant. *Adv. Mater.* **2020**, *32*, 2004210.

(9) Jiao, B.; Shi, A.; Wang, Q.; Binks, B. P. High-Internal-Phase Pickering Emulsions Stabilized Solely by Peanut-Protein-Isolate Microgel Particles with Multiple Potential Applications. *Angew. Chem., Int. Ed.* **2018**, *57*, 9274−9278.

(10) Crossley, S.; Faria, J.; Shen, M.; Resasco, D. E. Solid Nanoparticles that Catalyze Biofuel Upgrade Reactions at the Water/Oil Interface. *Science* **2010**, *327*, 68−72.

(11) Yang, H.; Fu, L.; Wei, L.; Liang, J.; Binks, B. P. Compartmentalization of Incompatible Reagents within Pickering Emulsion Droplets for One-Pot Cascade Reactions. *J. Am. Chem. Soc.* **2015**, *137*, 1362−1371.

(12) Wei, Q.; Yu, C.; Song, X.; Zhong, Y.; Ni, L.; Ren, Y.; Guo, W.; Yu, J.; Qiu, J. Recognition of Water-Induced Effects toward Enhanced Interaction between Catalyst and Reactant in Alcohol Oxidation. *J. Am. Chem. Soc.* **2021**, *143*, 6071−6078.

(13) Chen, Z.; Zhao, C.; Ju, E.; Ji, H.; Ren, J.; Binks, B. P.; Qu, X. Design of Surface-Active Artificial Enzyme Particles to Stabilize Pickering Emulsions for High-Performance Biphasic Biocatalysis. *Adv. Mater.* **2016**, *28*, 1682−1688.

(14) Chen, Z.; Zhou, L.; Bing, W.; Zhang, Z.; Li, Z.; Ren, J.; Qu, X. Light Controlled Reversible Inversion of Nanophosphor-Stabilized Pickering Emulsions for Biphasic Enantioselective Biocatalysis. *J. Am. Chem. Soc.* **2014**, *136*, 7498−7504.

(15) Li, Z.; Shi, Y.; Zhu, A.; Zhao, Y.; Wang, H.; Binks, B. P.; Wang, J. Light-Responsive, Reversible Emulsification and Demulsification of Oil-in-Water Pickering Emulsions for Catalysis. *Angew. Chem., Int. Ed.* **2021**, *60*, 3928−3933.

(16) Zeng, T.; Deng, A.; Yang, D.; Li, H.; Qi, C.; Gao, Y. Triple-Responsive Pickering Emulsion Stabilized by Core Cross-linked Supramolecular Polymer Particles. *Langmuir* **2019**, *35*, 11872−11880.

(17) Pera-Titus, M.; Leclercq, L.; Clacens, J.-M.; De Campo, F.; Nardello-Rataj, V. Pickering Interfacial Catalysis for Biphasic Systems: From Emulsion Design to Green Reactions. *Angew. Chem., Int. Ed.* **2015**, *54*, 2006−2021.

(18) Walther, A.; Hoffmann, M.; Müller, A. H. E. Emulsion Polymerization Using Janus Particles as Stabilizers. *Angew. Chem., Int. Ed.* **2008**, *47*, 711−714.

(19) Binks, B. P.; Murakami, R.; Armes, S. P.; Fujii, S. Temperature-Induced Inversion of Nanoparticle-Stabilized Emulsions. *Angew. Chem., Int. Ed.* **2005**, *44*, 4795−4798.

(20) Ren, G.; Zheng, X.; Gu, H.; Di, W.; Wang, Z.; Guo, Y.; Xu, Z.; Sun, D. Temperature and CO_2 Dual-Responsive Pickering Emulsions Using Jeffamine M2005-Modified Cellulose Nanocrystals. *Langmuir* **2019**, *35*, 13663−13670.

(21) Jiang, J.; Zhu, Y.; Cui, Z.; Binks, B. P. Switchable Pickering Emulsions Stabilized by Silica Nanoparticles Hydrophobized in Situ with a Switchable Surfactant. *Angew. Chem., Int. Ed.* **2013**, *52*, 12373−12376.

(22) Tu, F.; Lee, D. Shape-Changing and Amphiphilicity-Reversing Janus Particles with pH-Responsive Surfactant Properties. *J. Am. Chem. Soc.* **2014**, *136*, 9999−10006.

(23) Jiang, J.; Yu, S.; Zhang, W.; Zhang, H.; Cui, Z.; Xia, W.; Binks, B. P. Charge-Reversible Surfactant-Induced Transformation Between Oil-in-Dispersion Emulsions and Pickering Emulsions. *Angew. Chem., Int. Ed.* **2021**, *60*, 11793−11798.

(24) Geisel, K.; Isa, L.; Richtering, W. The Compressibility of pH-Sensitive Microgels at the Oil–Water Interface: Higher Charge Leads to Less Repulsion. *Angew. Chem., Int. Ed.* **2014**, *126*, 5005−5009.

(25) Lam, S.; Blanco, E.; Smoukov, S. K.; Velikov, K. P.; Velev, O. D. Magnetically Responsive Pickering Foams. *J. Am. Chem. Soc.* **2011**, *133*, 13856−13859.

(26) Peng, J.; Liu, Q.; Xu, Z.; Masliyah, J. Synthesis of Interfacially Active and Magnetically Responsive Nanoparticles for Multiphase Separation Applications. *Adv. Funct. Mater.* **2012**, *22*, 1732−1740.

(27) Sun, H.; Li, M.; Li, L.; Liu, T.; Luo, Y.; Russell, T. P.; Shi, S. Redox-Responsive, Reconfigurable All-Liquid Constructs. *J. Am. Chem. Soc.* **2021**, *143*, 3719−3722.

(28) Zhu, Y.; Jiang, J.; Liu, K.; Cui, Z.; Binks, B. P. Switchable Pickering Emulsions Stabilized by Silica Nanoparticles Hydrophobized *in Situ* with a Conventional Cationic Surfactant. *Langmuir* **2015**, *31*, 3301−3307.

(29) Chen, Y.; Li, Z.; Wang, H.; Pei, Y.; Shi, Y.; Wang, J. Visible Light-Controlled Inversion of Pickering Emulsions Stabilized by Functional Silica Microspheres. *Langmuir* **2018**, *34*, 2784−2790.

(30) Kosif, I.; Cui, M.; Russell, T. P.; Emrick, T. Triggered In situ Disruption and Inversion of Nanoparticle-Stabilized Droplets. *Angew. Chem., Int. Ed.* **2013,** *52*, 6620−6623.

(31) Shi, S.; Russell, T. P. Nanoparticle Assembly at Liquid–Liquid Interfaces: From the Nanoscale to Mesoscale. *Adv. Mater.* **2018,** *30*, 1800714.

(32) Chai, Y.; Hasnain, J.; Bahl, K.; Wong, M.; Li, D.; Geissler, P.; Kim, P. Y.; Jiang, Y.; Gu, P.; Li, S.; Lei, D.; Helms, B. A.; Russell, T. P.; Ashby, P. D. Direct observation of nanoparticle-surfactant assembly and jamming at the water-oil interface. *Sci. Adv.* **2020**, *6*, eabb8675.

(33) Huang, C.; Sun, Z.; Cui, M.; Liu, F.; Helms, B. A.; Russell, T. P. Structured Liquids with pH-Triggered Reconfigurability. *Adv. Mater.* **2016**, *28*, 6612−6618.

(34) Huang, C.; Chai, Y.; Jiang, Y.; Forth, J.; Ashby, P. D.; Arras, M. M. L.; Hong, K.; Smith, G. S.; Yin, P.; Russell, T. P. The Interfacial Assembly of Polyoxometalate Nanoparticle Surfactants. *Nano Lett.* **2018**, *18*, 2525−2529.

(35) Yamase, T. Photo- and Electrochromism of Polyoxometalates and Related Materials. *Chem. Rev.* **1998**, *98*, 307−326.

(36) Yamase, T. Photochemical studies of alkylammonium molybdates. Part 9. Structure of dimagnetic blue species involved in the photoredox reaction of $[Mo_7O_{24}]^{6-}$. *J. Chem. Soc., Dalton Trans.* **1991**, *301*, 3055−3063.

(37) Pope, M. T.; Müller, A. Polyoxometalate Chemistry: An Old Field with New Dimensions in Several Disciplines. *Angew. Chem., Int. Ed.* **1991**, *30*, 34−48.

(38) Zou, W.; González, A.; Jampaiah, D.; Ramanathan, R.; Taha, M.; Walia, S.; Sriram, S.; Bhaskaran, M.; Dominguez-Vera, J. M.; Bansal, V. Skin color-specific and spectrally-selective naked-eye dosimetry of UVA, B and C radiations. *Nat. Commun.* **2018**, *9*, 3743.

(39) Wang, H.; Hamanaka, S.; Nishimoto, Y.; Irle, S.; Yokoyama, T.; Yoshikawa, H.; Awaga, K. In Operando X-ray Absorption Fine Structure Studies of Polyoxometalate Molecular Cluster Batteries: Polyoxometalates as Electron Sponges. *J. Am. Chem. Soc.* **2012**, *134*, 4918−4924.

(40) Yao, J. N.; Hashimoto, K.; Fujishima, A. Photochromism induced in an electrolytically pretreated MoO_3 thin film by visible light. *Nature* **1992**, *355*, 624−626.

(41) Zhang, G.; Yang, W.; Yao, J. Thermally Enhanced Visible-Light Photochromism of Phosphomolybdic Acid–Polyvinylpyrrolidone Hybrid Films. *Adv. Funct. Mater.* **2005**, *15*, 1255−1259.

(42) Fan, J.; Bao, B.; Wang, Z.; Li, H.; Wang, Y.; Chen, Y.; Wang, W.; Yu, D. Flexible, switchable and wearable image storage device based on light responsive textiles. *Chem. Eng. J.* **2021**, *404*, 126488.

(43) Yang, R. T.; Hernández-Maldonado, A. J.; Yang, F. H. Desulfurization of Transportation Fuels with Zeolites Under Ambient Conditions. *Science* **2003**, *301*, 79−81.

(44) Kim, K.; Kim, S.; Ryu, J.; Jeon, J.; Jang, S. G.; Kim, H.; Gweon, D. G.; Im, W. B.; Han, Y.; Kim, H., Ryu, J. Processable high internal phase Pickering emulsions using depletion attraction. *Nat. Commun.* **2017**, *8*, 14305.

(45) Viswanathan, P.; Chirasatitsin, S.; Ngamkham, K.; Engler, A. J.; Battaglia, G. Cell Instructive Microporous Scaffolds through Interface Engineering. *J. Am. Chem. Soc.* **2012**, *134*, 20103−20109.

(46) Ikem, V., Menner, A., Bismarck, A. High Internal Phase Emulsions Stabilized Solely by Functionalized Silica Particles. *Angew. Chem., Int. Ed.* **2008**, *47*, 8277−8279.

(47) Wu, B., Yang, C., Xin, Q., Kong, L., Eggersdorfer, M., Ruan, J., Zhao, P., Shan, J., Liu, K., Chen, D., Weitz, D. A., Gao, X. Attractive Pickering Emulsion Gels. *Adv. Mater.* **2021**, *33*, 2102362.

(48) Williams, J. M.; Wrobleski, D. A. Spatial distribution of the phases in water-in-oil emulsions. Open and closed microcellular foams from cross-linked polystyrene. *Langmuir* **1988**, *4*, 656−662.
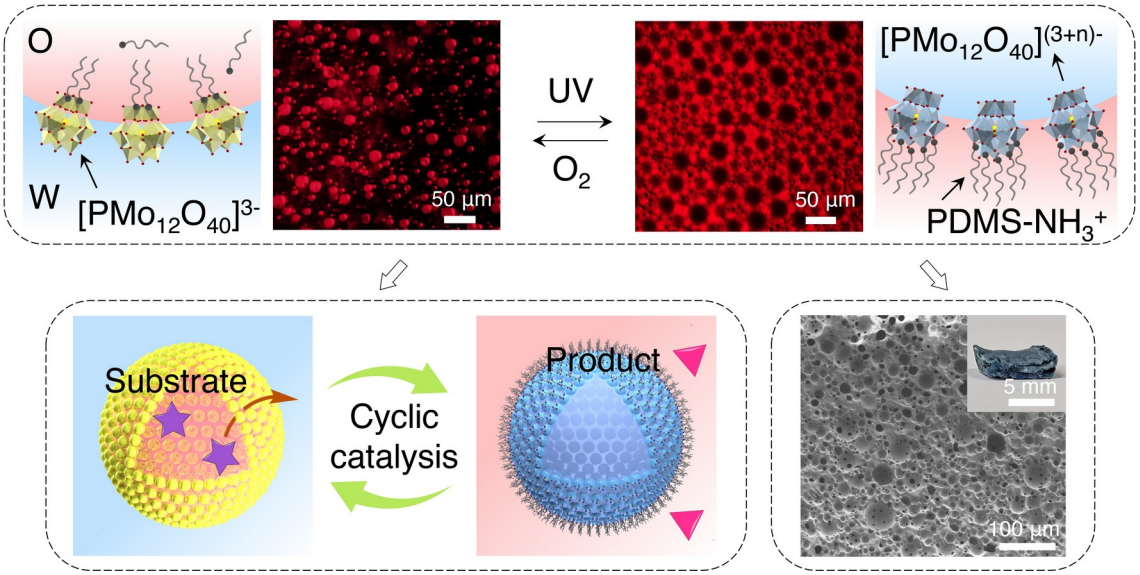
For Table of Contents Only